Preferred orientations and stability of medium length *n*-alkanes solidified in mesoporous silicon

A. Henschel, T. Hofmann, P. Huber,* and K. Knorr†
Technische Physik, Universität des Saarlandes, D-66041 Saarbrücken, Germany
(Received 26 October 2006; published 26 February 2007)

The *n*-alkanes $C_{16}H_{34}$, $C_{17}H_{36}$, $C_{19}H_{40}$, and $C_{25}H_{52}$ have been imbibed and solidified in mesoporous, crystalline silicon with a mean pore diameter of 10 nm. The structures and phase sequences have been determined by x-ray diffractometry. Apart from a reduction and the hysteresis of the melting-freezing transition, we find a set of six discrete orientation states ("domains") of the confined alkane crystals with respect to the lattice of the silicon host. The growth process responsible for the domain selection is interpreted as a nanoscale version of the Bridgman technique known from single-crystal growth. Oxidation of the pore walls leads to extrusion of the hydrocarbons upon crystallization, whereas the solidified *n*-alkanes investigated in nonoxidized, porous silicon are thermodynamically stable.

DOI: 10.1103/PhysRevE.75.021607 PACS number(s): 81.10.−h, 61.46.Hk, 61.10.−i, 68.18.Jk

I. INTRODUCTION

Molecular ensembles embedded in mesopores have properties different from those of the bulk condensed state. It has been known for a long time that the melting-freezing temperature is strongly affected by pore confinement [1,2]. For Ar in the 7 nm pores of Vycor glass, a standard mesoporous matrix, a downward shift of about 9% and a thermal hysteresis between freezing and melting has been observed [3]. The medium length *n*-alkane $C_{19}H_{40}$ (C19) in a "controlled pore glass" with about the same pore diameter shows an analogous behavior, not only for the freezing-melting transition but also for the subsequent transition from the so-called rotator mesophase R_I to the low-*T* "crystalline" *C* phase [4].

As for the crystallographic structure of the solidified pore filling, it appears that there is on the whole little difference with respect to the bulk state, at least when concentrating on small molecules and leaving aside the fraction of the material placed next to the pore walls. Thus pore condensates of Ar or O_2 crystallize in the structures and with the lattice parameters known from the bulk systems [3,5]. The situation for the normal alkanes is somewhat different. In the bulk state these rodlike molecules form layered crystals—see inset of Fig. 1. For the medium length odd alkanes the molecular axes are oriented normal to the layers. The low-*T C* phase of such systems is orthorhombic *Pbcm* with a bilayer-type stacking of the layers. Thus the lattice parameter *c* is about twice the length of the molecules that are in an extended all-*trans* configuration. Within the layers the structure can be understood as a close packed, slightly uniaxially compressed hexagonal array of molecules lying side by side. The deviation *D* of the ratio of the lattice parameters *a* and *b* from the value of $\sqrt{3}$ is a measure of this distortion, $D=1-a/b\sqrt{3}$. In even-numbered alkanes the molecular axes are tilted with respect to the layers, leading to a triclinic *P* structure at low *T*. Close to the melting point mesophases appear in which there is partial or complete disorder of the molecules with respect to the orientation about their long axis. The R_{II} phase is hexagonal due to complete azimuthal disorder; in the orthorhombic *Fmmm* R_I phase the molecules can flip between two azimuthal orientations; here the layers are still uniaxially deformed with respect to the hexagonal reference. The medium length even alkanes do not have mesophases; they crystallize directly into the triclinic phase [6–10].

In our previous x-ray diffraction study on pore confined C19, the in-plane diffraction pattern has been shown to be close to that of the bulk state, but the layering reflections were absent, due to a suppression of the lamellar order. Furthermore, a second rotator phase R_{II}, in addition to the R_I phase and absent in the bulk state of this alkane, appeared right at the melting point [4]. The pore confined even alkanes C14 and C16 show an intermediate R_I phase which does not occur in the bulk state of these molecular solids [11]. Analogous observations have been made for medium length *n*-alkanes spatially confined in emulsified *n*-alkane microdroplets [12], microcapsules [13], and nanochannels of the

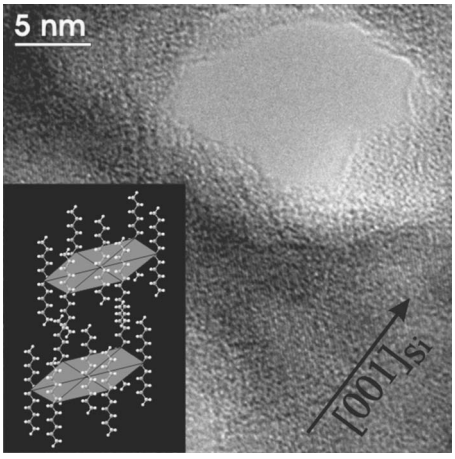

FIG. 1. Transmission electron microscopy picture of a mesopore in porous silicon. The light gray area and the dark gray regions represent the pore entrance and the pore walls, respectively. The picture is taken along the $[100]_{Si}$ direction of the Si lattice, which agrees with both the surface normal of the porous sheet and the long axis of the tubular pores. The $[001]_{Si}$ crystallographic direction of Si is indicated by an arrow. Inset: Schematic view of an *n*-alkane crystal.

*Electronic address: p.huber@physik.uni-saarland.de
†Electronic address: knorr@mx.uni-saarland.de

template-grown mesoporous silica matrix MCM-41 [14].

In the present paper we reinvestigate the structure of medium length *n*-alkanes in mesopores and present results on the odd alkanes C17, C19, C25, and on the even alkane C16. The main difference with respect to our previous studies refers to the substrate. The porous glasses used so far have randomly oriented pores. Thus the diffraction patterns of the pore fillings are always powder patterns in the crystallographic sense, even if there were preferred crystallographic orientations of the pore filling with respect to the pore axis. Porous Si on the other hand maintains the single-crystalline character of the Si wafer from which it is made, and furthermore the pores are all parallel and normal to the (100) surface of the wafer. This gives access to the orientation of the alkane lattice with respect to the Si lattice and thereby with respect to the pore axis. In fact we will demonstrate that the alkanes solidified in the porous Si show a set of discrete orientation states ("domains"). This substrate offers a second advantage. The chemistry of the substrate and thereby the strength of the alkane-substrate interaction can be easily changed by subsequent oxidation of the pore walls [15–17].

II. EXPERIMENT

Pores were electrochemically etched into the surface of a Si (100) wafer according to a standard recipe [18]. After the porous layer reached the desired thickness of 70 μm, the anodization current was increased by a factor of 10 with the result that the porous layer is released from the bulk wafer underneath. The analysis of a vapor pressure isotherm of Ar at 86 K suggests that the pore diameter is of the order of 10 nm and the porosity about 50%. The single-crystalline state of the porous sheet has been checked by x-ray and electron diffraction. Note, however, that the sheet is slightly warped with a variation of the sheet normal of 6° when scanning across the surface.

The sample is imbibed by bringing it in contact with the liquified alkane. Bulk excess material outside the pores is removed with paper tissue. The sample is mounted on a frame in the sample cell. The cell consists of a Peltier cooled base plate and a Be cap. It is filled with He gas for thermal contact. The cell is in a vacuum chamber, the outer jacket of which has Mylar windows allowing the passage of the x rays over a wide range of scattering angles within the scattering plane but allows practically no tilt with respect to the scattering plane. The lowest temperature reachable with the setup is $T=245$ K.

The diffraction experiments have been carried out on a two-circle diffractometer with graphite monochromatized Cu K_α radiation emanating from a rotating anode. The two angles that can be varied are the detector angle 2Θ and the rotation angle ω about the normal of the scattering plane. The sample is mounted perpendicular, such that the [100] sheet normal and the [011] direction of the Si lattice lie in the scattering plane. Introducing the rotation angle χ about the sheet normal (i.e., the rotation of the porous sheet on the frame to which it is clamped), this standard orientation of the sample defines the zero value of χ. The scattering plane with the relevant components of the momentum transfer q_p and q_s parallel and perpendicular to the pore axes is shown in Fig. 2. Φ is the azimuth within the scattering plane, measured from the pore axis.

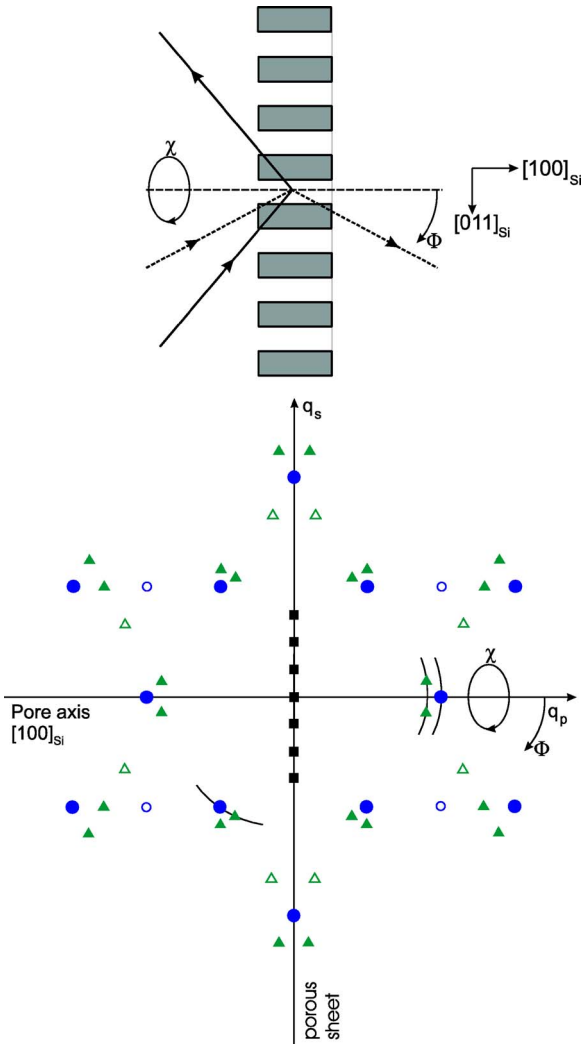

FIG. 2. (Color online) The scattering plane in direct (top) and reciprocal (bottom) space. The porous sheet is mounted perpendicular to the scattering plane. q_p and q_s are the wave vector components parallel and perpendicular to the pore axis, which in turn is parallel to the $[100]_{Si}$ direction of the Si lattice. The angular variables Φ and χ are indicated. For $\chi=0$, $[011]_{Si}$ lies in the scattering plane. Also shown are the incoming and the outgoing x-ray beams for a scan along q_p (bisecting reflection geometry) and along q_s (transmission). The Bragg peaks of the six orthorhombic domains are shown in the lower panel. Included are peaks with $2\Theta<40°$ that lie in the plane and slightly above or below the plane (within the reach of the vertical divergence of the diffraction setup). The inner ring represents orthorhombic peak triples originating from the splitting of the $\{100\}_{hex}$ reflections of the hexagonal reference lattice, peaks of the outer ring from $\{110\}_{hex}$, and peaks of the intermediate ring are superlattice reflections of the *C* phase. The layering reflections of the $\chi=90°$ domains are shown by squares. Circles and triangles distinguish peaks of the majority and minority Φ domains.

The samples have been systematically studied as a function of T by performing radial 2Θ-ω scans along q_p and q_s. That is $\omega=\Theta+\Phi$ with $\Phi=0$ for scans along q_p and $\Phi=90°$

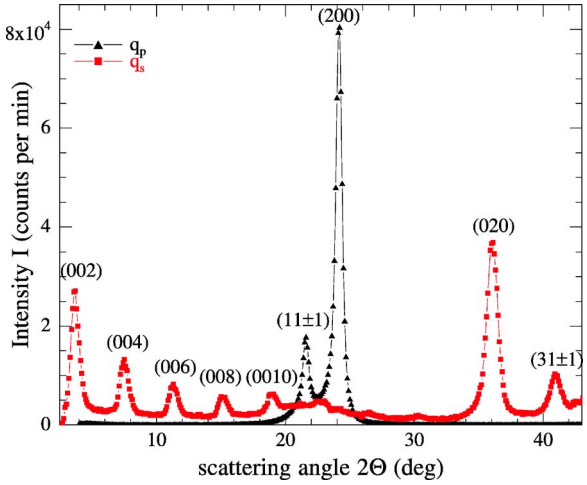

FIG. 3. (Color online) The profiles of radial scans along q_p and along q_s on C17 at 245 K. A background obtained with empty pores has been subtracted. The counting rates of the q_s scan have been multiplied by a factor of 5.

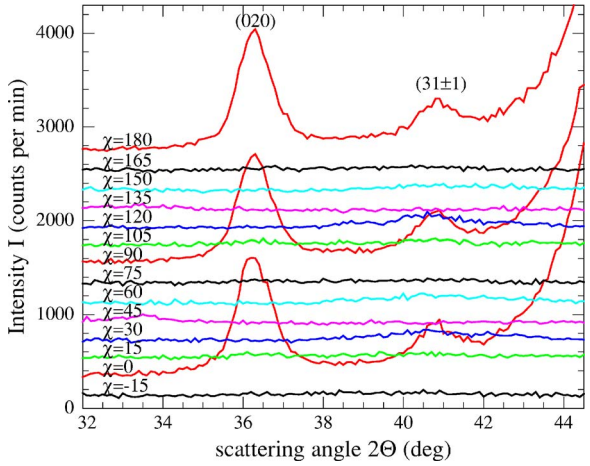

FIG. 4. (Color online) Sections of q_s scans on C25 at 290 K performed upon varying the angle χ from −15° to 180° in steps of 15°. The profiles are shifted vertically by equal amounts. For χ =0°, 90°, and 180°, the (020) and the (311)-(31$\bar{1}$) peaks and the low-2Θ wing of the $(022)_{Si}$ peak appear.

for scans along q_s, corresponding to reflection and transmission geometry, respectively. The modulus of the scattering vectors q_s and q_p is given by $q_{s,p}=4\pi/\lambda \sin\Theta$, where $\lambda = 1.5418$ Å^{-1}. Stronger reflections of the pore fillings are confined to 2Θ values below 50°, in agreement with our previous studies on alkanes in porous glasses. Occasionally rocking scans (Φ scans) were performed. In reflection geometry the span of such scans is very limited, since very soon a situation is reached in which the in- or the outgoing beam is parallel to the sample. In this case the absorption of the x rays in the sample depends strongly on Φ.

In a separate experiment the variation of the intensity of selected diffraction peaks of C25 was studied as function of the rotation angle χ about the pore axis. For this purpose the sample was clamped on a rotatory support and χ was varied in steps of 15°. These measurements were performed at room temperature only (at which C25 is already solid).

Even though the setup used does not allow us to record complete pole figures, the information obtained is sufficient to identify the peculiar texture of the solidified pore fillings.

III. DIFFRACTION RESULTS

The diffraction results cannot be explained in terms of powder patterns. This is demonstrated in Figs. 3 and 4.

The patterns of Fig. 3 are obtained on C17 with $\chi=0$ by means of radial scans along q_p and q_s, respectively. In the case of a powder pattern, these scans should be identical apart from different scale factors and slow variations of the intensity with 2Θ due to different path lengths of the x-ray beam through the sample, but obviously they depend strongly on the in-plane azimuth Φ. Thus, e.g., the layering reflections (001) are present in transmission but absent in reflection geometry. The diffraction pattern also depends on the angle χ; intense alkane reflections have been obtained for χ a multiple of 90° only.

See Fig. 4 for q_s scans on C25. In fact, the peak intensities are by at least one order of intensity stronger than what we have observed previously on alkanes in porous glasses [4].

We start from the idea that the results can be explained in terms of six discrete orientation states of the alkane lattice with respect to the Si lattice. The reference phase of the alkanes is the orthorhombic low-T phase C with a bilayer AB stacking scheme. We postulate that upon solidification the alkanes pass through a (real or virtual) hexagonal parent phase with one of the $\{100\}_{hex}$ fundamental reciprocal lattice vectors parallel to the pore axis, and that the subsequent uniaxial compression that appears at the hexagonal-orthorhombic transition is along one of these lattice vectors. Thereby three Φ domains are established, with the orthorhombic a direction forming angles of 0 and ±60° with the pore axis. The Φ=0 domain turns out to be the majority domain. Here the uniaxial distortion D is along the pore axis. The normal of the alkane layers is then perpendicular to the pore axis and the experiments show that it is parallel either to the [011] or to the [0$\bar{1}$1] direction of the Si lattice. Thus there are two discrete χ states, $\chi=0$ and $\chi=90°$. This leads to six domains in total. In Fig. 2 we show the low-2Θ alkane reflections that are expected to lie in or at least close to the scattering plane when all six orientation states are present. This texture explains not only why the layering reflections (001) can be seen in radial q_s scans only, but also why the orthorhombic products of the fundamental $\{100\}_{hex}$ and of the first overtone $\{110\}_{hex}$ hexagonal in-plane reflections occur in orthogonal scan directions.[1]

Some complementary rocking scans (Φ scans) have been performed.

In Fig. 5 examples on C17 that probe the peaks that result from the splitting of the $\{100\}_{hex}$ fundamental reflections of the hexagonal parent lattice are shown. See Fig. 2 for the scan paths. Whenever it appeared appropriate, the scan profiles were decomposed into two components, accounting

[1]See also [6] for the reciprocal lattice of various crystallographic phases of the alkanes.

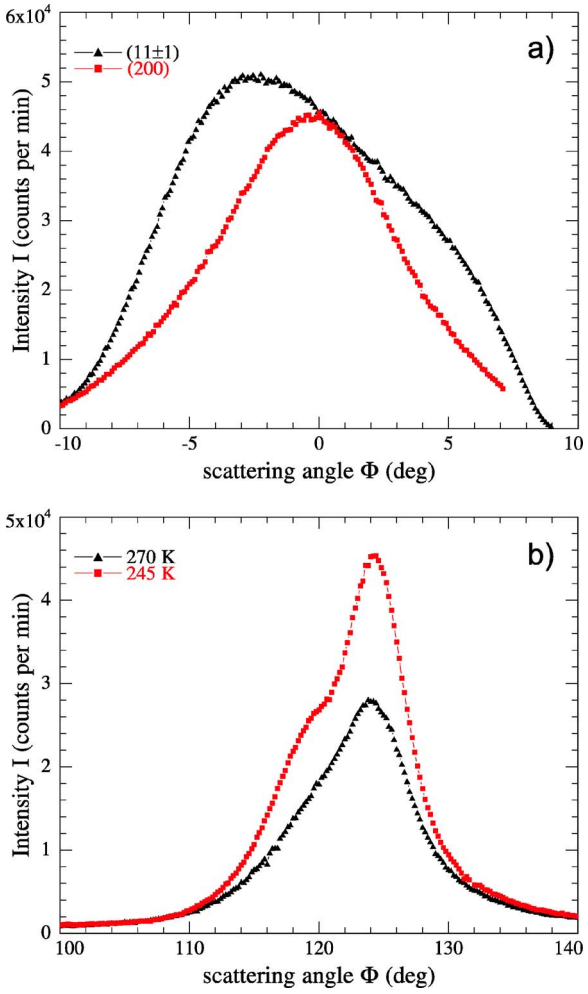

FIG. 5. (Color online) Profiles of rocking scans on C17. The scans shown in (a) have been taken at 263 K; they probe the (111)-(11$\bar{1}$) and the (200) reflection, respectively. The scans of (b) probe the two inner peaks of the peak triple centered at $\Phi=120°$. One scan has been recorded at 270 K, the other at 245 K. The scan paths are indicated in Fig. 2.

properly for the finite Φ width and correcting for the Φ-dependent absorption. About the same relatively large Φ width has been observed in rocking scans of Si reflections. Thus, the width stems from the warping of the porous sheet and not from a mosaic width of the alkane lattice with respect to the Si lattice.

One scan of Fig. 5(a) crosses the (200) reflection (Miller triples without subscript refer to the orthorhombic lattice). This peak lies in the scattering plane and is centered at $\Phi=0$. According to the domain model of Fig. 2, it originates from the $\Phi=0$ and $\chi=0$ and 90° domains. The second scan of Fig. 5(a) probes the (111)-(11$\bar{1}$) pair of reflections of the $\Phi=\pm 60°$, $\chi=90°$ domains. These reflections are slightly above and below the scattering plane at a distance that is proportional to the orthorhombic strain D. Their finite intensity along the scan path stems from the vertical divergence of the scattering setup and from the warping of the sample sheet. The pair is centered at $\Phi_0=\pm(6\pm1)°$. This value is consistent with the AB stacking scheme of the alkane layers in the orthorhombic phase. In contrast to the situation in the porous glasses, the confinement in porous Si leaves the layered structure of the alkanes intact, as can be seen already from the (001) layering reflections, and even conserves the bilayer type stacking. If, e.g., the layers stacked randomly, i.e., with no lateral correlation between layers, the third Miller index l of the (111)/(11$\bar{1}$) reflections would be irrelevant and the scan profile of Fig. 5(a) should mimic the form factor of the molecule along the (11) Bragg rod.

The Bragg peaks (200) and (111)-(11$\bar{1}$) tested by the scans of Fig. 5(a) come from different domains. At the temperature chosen, $T=263$ K, the peaks and therefore the domains have about equal weights. The scans of Fig. 5(b) cross the two inner peaks of an equivalent peak triplet centered at $\Phi=120°$ (see Fig. 2). Here the stacking scheme, via the Miller index l, has negligible effect on the peak positions; the splitting arises almost exclusively from the uniaxial distortion D within the layers. At 270 K, D is still small and the splitting cannot be resolved. At 245 K, the lowest temperature of our setup, D has grown to such a value that the peaks can be separated. According to Fig. 2, the two components represent the $\Phi=0$ "majority" domain and one of the $\Phi=\pm 60°$ "minority" domains. By the time this temperature is reached on cooling, the majority domain has gained a statistical weight about twice that of the minority domain. Obviously the domains rearrange upon changes of temperature.

The orthorhombic lattice parameters a,b,c can be derived from the 2Θ positions of the diffraction peaks of the radial scans along q_p and q_s. The layering peaks (001) show up in scans along q_s ($l=2n$, because of the bilayer-type stacking). Within the experimental resolution, the lattice parameter c of the odd alkanes studied is independent of T and has the values known from the bulk systems [6–9] (see below for C16). The intrinsic radial width of the layering peaks is independent of the node index l, indicating that the peak broadening is due to finite size. A coherence length of 11 nm is obtained, a value that is comparable to the pore diameter. According to the domain model the pore diameter is an upper bound for the size of the crystallites along the c direction.

The in-plane lattice parameters a and b can be extracted from the positions of the reflections (111)-(11$\bar{1}$) and (200) of the q_p scan and of the higher-order reflections (020) and (311)-(31$\bar{1}$) of the q_s scan. See Fig. 3 for the results of the two scan directions on C17 at 245 K and Fig. 6 for the T dependence of the (111)-(11$\bar{1}$) and (200) doublet of all four alkanes investigated.

Since our diffraction setup does not allow a precise measurement of the absolute values of the lattice parameters, we do not give absolute values but concentrate on the uniaxial distortion D, $D=1-a/b\sqrt{3}$. D is accessible from the peak splittings and thereby the influence of systematic errors is reduced. For all alkanes investigated the data on the pore confined material agree roughly with the data on the bulk systems [8,9] when allowing for a shift ΔT in temperature of 12 to 15 K. In Fig. 7 one can find three representative $D(T)$ dependences, i.e., of confined C16, C17, and C25.

In Fig. 6 we show the (111)-(11$\bar{1}$) and (200) profile at some selected temperatures of cooling cycles as probed by

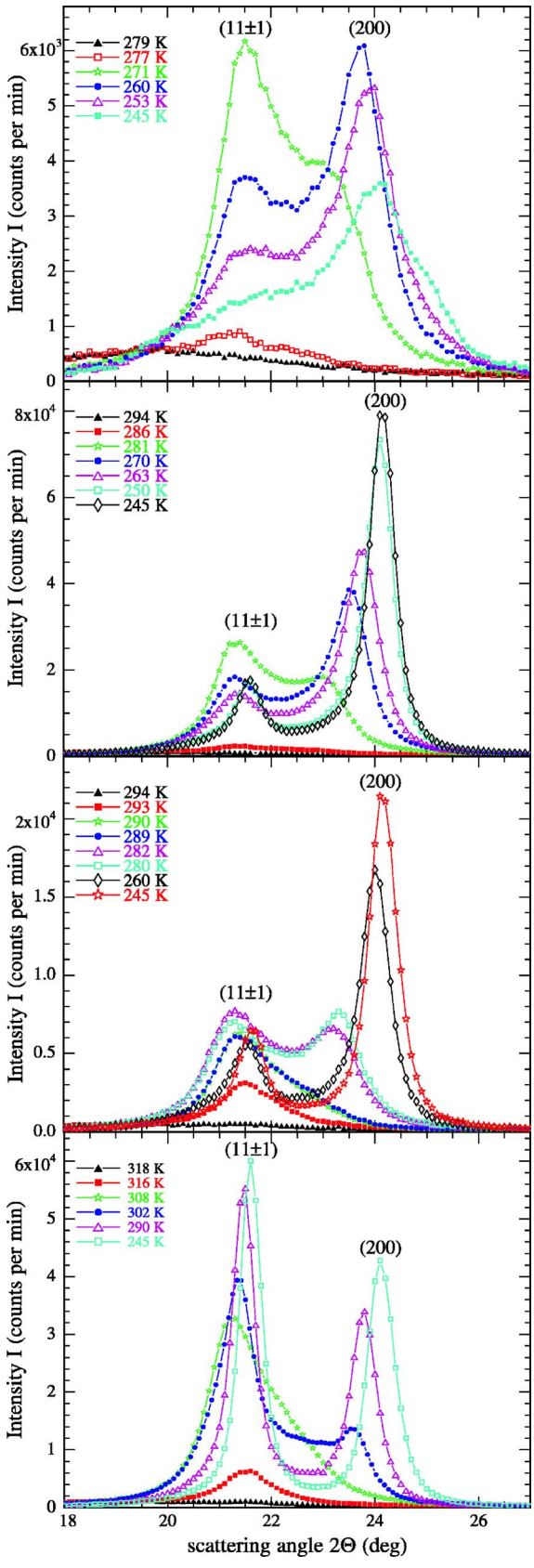

FIG. 6. (Color online) Profiles of q_p scans showing the (111)-(11$\bar{1}$) and (200) doublet at selected temperatures of cooling cycles on the four alkanes investigated in this study. From top to bottom C16, C17, C19, and C25.

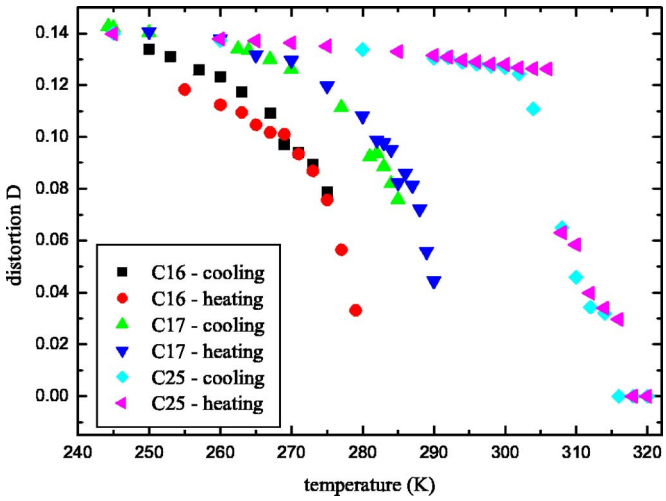

FIG. 7. (Color online) The temperature dependence of the uniaxial distortion D, on both cooling and heating, of C16, C17, and C25.

radial scans along q_p. The first appearance of Bragg intensity on cooling signals freezing, its disappearance on heating melting. The pore freezing and melting temperatures T_f and T_m are listed in Table I. Right after solidification the two peaks overlap. As D increases on cooling, the (111)-(11$\bar{1}$) and (200) splitting develops. At higher temperatures within the solid regime the intensity ratio r is in favor of the (111)-(11$\bar{1}$) peak, $r>1$, but at lower temperature this ratio is reversed in favor of the (200) peak, $r<1$, for C16, C17, and C19 (but not for C25). These intensity changes are by far larger than what can be explained by changes of the structure factors upon orientational ordering. The (200) Bragg point is directly crossed by the q_p scan. Its intensity increase is in first respect due to an increase of the statistical weight of the majority domain. For the (111)-(11$\bar{1}$) reflection the situation is more complex. Three aspects have to be considered, which are difficult to separate with just q_p scans at hand. From what has been said on the majority domain it is clear that the decrease of r is to some part due to a decrease of the statistical weight of the minority domains, but one also has to realize that the (111)-(11$\bar{1}$) peaks are not centered on but rather displaced from the scan path such that only their wings contribute to the intensity of a q_p scan. One component of the displacement is within the scattering plane, it

TABLE I. The pore freezing and melting temperatures T_f and T_m of the alkanes in porous Si (in K) as given by the onset of Bragg intensities on cooling and their disappearance on heating. The error is 1 K. The melting temperatures of the bulk state are included for comparison [19,20].

Alkane	Bulk	T_f	T_m
C16	291	277	283
C17	295	286	291
C19	305	293	297
C25	327	316	322

depends on the stacking scheme of the alkane layers, the other component is perpendicular to the scattering plane and scales with the distortion D. Thus the values of $r<1$ observed for C17 and C19 at lower T suggest a well developed uniaxial distortion D in combination with a bilayer-type stacking. In case of vanishing distortion D, equal domain weights, and random stacking, the intensity ratio r should be close to 2, simply reflecting the multiplicities of the peaks involved, and in fact r values of this order are observed at higher T. This indicates that close to the freezing-melting transition the AB stacking scheme is heavily perturbed or perhaps even completely randomized by stacking faults. For C25, the longest alkane studied, r remains close to 2 down to the low-T limit of our experiment. Obviously C25 has the largest number of stacking faults. This appears plausible since stacking faults are induced by gauche defects, the probability of which increases with the chain length [21].

Translating the radial width of the (200) peak into a coherence length along the pore axis, one obtains a value of about 25 nm. The actual size of the crystallites in this direction may be in fact even larger since the width of this reflection is likely to be affected additionally by strains.

The even-numbered alkane C16 is a special case. Below the freezing temperature the peak doublet observed along q_p evolves in the same way as for odd alkanes C17 and C19 (Figs. 5 and 6). This remarkable observation has already been made for C16 in Vycor glass. Obviously C16 in nanometer pores shows a mesophase of orthorhombic structure (C or more likely R_I) with the molecules oriented perpendicular to the layers. Such a phase does not appear in the bulk state of this molecule [22]. Below about 270 K down to the minimum temperature of the setup, further changes occur that we interpret in terms of an incomplete change into the triclinic low-T phase that is known from the bulk system. In particular, an additional reflection shows up as shoulder on the high-2Θ wing of the (200) peak, at a 2Θ value consistent with the strongest reflection of the triclinic phase. This phase transformation from orthorhombic to triclinic involves a tilting of the molecules that in turn leads to a slight reduction of the layer thickness, the repeat unit along c that is accessible from the (00l) positions (see Fig. 8).

Both the in-plane lattice parameters (see Fig. 7 for the uniaxial distortion D) and the layer thickness show some hysteresis between heating and cooling, indicating that the transformation is hysteretic. Figure 8 suggests that the transformation starts at about 260 K, that at 245 K about 30% of the material has transformed into the triclinic phase, and that on heating the orthorhombic mesophase is completely restored only a few degrees short of T_m. See our work on C14 and C16 in Vycor for more information on the orthorhombic-triclinic transformation of even-numbered alkanes in mesopores [11].

Bragg peaks of the type (21l) are superlattice reflections of the C with respect to the R_I phase; they probe the low-T herringbone pattern of orientational ordering. At lower temperatures, a peak appears in q_s scans on the odd alkanes that can be indexed (210); see Fig. 9 for results on C25. Thus the pore confined odd alkanes eventually transform into the low-T C phase at some temperature larger than 245 K. The intensity of this peak is, however, low and it is difficult to extract

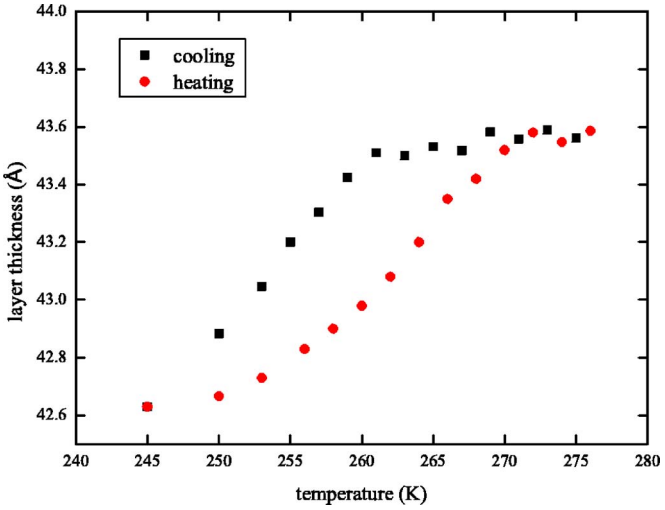

FIG. 8. (Color online) The layer thickness of C16 as function of temperature, on both cooling and heating.

reliable values of the C-R_I transition temperatures. Not only is the structure factor of the superlattice reflections more than one order of magnitude smaller than that of the fundamental reflections, but it is also clear from Fig. 2 that the (210) reflections come from the minority domains and that the q_s scan picks up the wings of these reflections only.

IV. DOMAIN SELECTION PROCESS

Of course it is not the complete pore filling that exists as discrete orientation states. There is, e.g., an increased background in the q_s scan of Fig. 3 in the 2Θ range of the (111)-(11$\bar{1}$) and (200) doublet. This is also the range of the first maximum of the structure factor of the liquid state of the alkanes. Hence there is a small liquidlike or amorphous component existing next to the rough pore walls, in niches. Occasionally even (111)-(11$\bar{1}$) and (200) peaks could be ob-

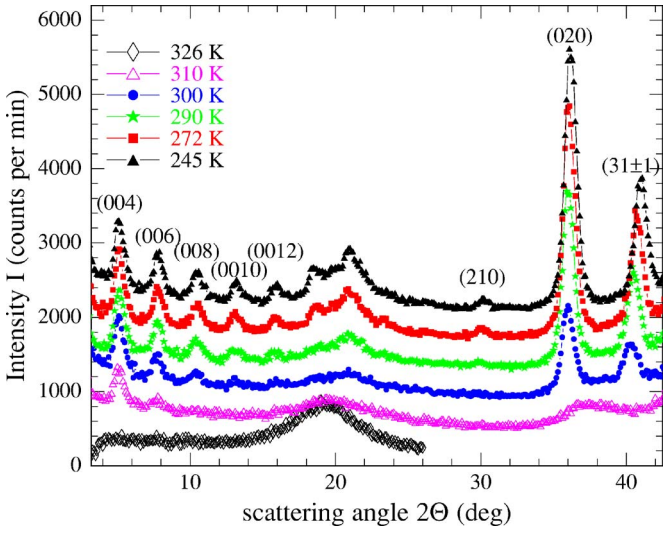

FIG. 9. (Color online) Profiles of q_s scans on C25 at selected temperatures.

served in q_s scans (Fig. 9) representing crystallites that do not obey the domain rule, but their intensities are much smaller than in q_p scans. Considering the different absorption of the x rays in the two scattering geometries one arrives at the estimate that at least 80% of the crystalline part of the pore filling exists in the form of the six domains.

How does this texture come out? The hcp solid state of N_2 in porous Si has been prepared in two ways, by the sublimation of vapor into the pores and, alternatively, by imbibing the liquid and subsequent solidification by cooling. In the second case there is strong texture with the hexagonal c axis preferentially aligned along the pore axis, whereas in the first case the orientational distribution of the hexagonal lattice is isotropic, giving rise to powder-type diffraction patterns [23]. Obviously texture is brought forth by the propagation of the solidification front along a special crystallographic direction. A crystalline nucleus is doomed to grow to large size when the growth direction coincides with the pore axis. The Bridgman technique of single-crystal growth relies on this selection process. Given the strong intermolecular binding within the alkane lamellae and the weaker binding across the gap between the lamellae, the maximum growth speed is expected to occur in a lateral direction. Furthermore, crystallization presumably occurs by adding close packed rows of molecules. Thus the propagation vector of solidification is along one of the principal wave vectors $\{100\}_{hex}$ of the quasihexagonal alkane lattice. Those crystallites grow and finally prevail that have such a vector along the pore axis. This also means that the layer normal and the long axis of the molecules are perpendicular to the pores axis. The orthorhombic a direction can be parallel to any one of these directions and therefore three Φ states result. Obviously the $\Phi=0$ domain finally dominates, its statistical weight increases as the uniaxial deformation D increases on cooling.

The χ texture is imposed by the fact that the pore axis is along the fourfold [100] direction of the Si lattice. The alkane layers are parallel to the (011) or to the $(0\bar{1}1)$ plane of the Si lattice. This may appear plausible in case the pore walls were preferentially of this type. We have recorded some electron microscope pictures of the porous Si sheet (Fig. 1). Indeed, the pores are by no means circular but have an irregular more or less polygonal cross section, but with no obvious preference for the pore walls to be (011) or $(0\bar{1}1)$ facets.

On the other hand these facets are prominent cleavage planes of Si crystals. In any case the diffraction results leave no doubt that there is again selection by growth starting from crystalline nuclei that have the lamellae parallel to such facets. A schematic picture of the crystallization of the alkanes in the pores is presented in Fig. 10.

What favors the $\Phi=0$ domains at lower T? The contraction of the orthorhombic alkane lattice on cooling is mainly along a; b is practically independent of T. Obviously an orientation of the crystallites is favored in which their T-independent dimension along b is clamped between opposite pore walls and the direction of maximum contraction is along the pore axis.

V. STABILITY OF THE PORE FILLING

A drop of liquid alkane is sucked into the pores. The chemical potential of the pore liquid is lower than that of the bulk liquid. This is due to the fact that the alkane-substrate interaction is stronger than the intermolecular interaction. It is by no means obvious that the pore solid is stable, too, since the matching of the crystal lattice of the solidified pore filling to the pore geometry costs some strain energy in form of lattice defects, grain boundaries in particular, that are absent in the liquid state.

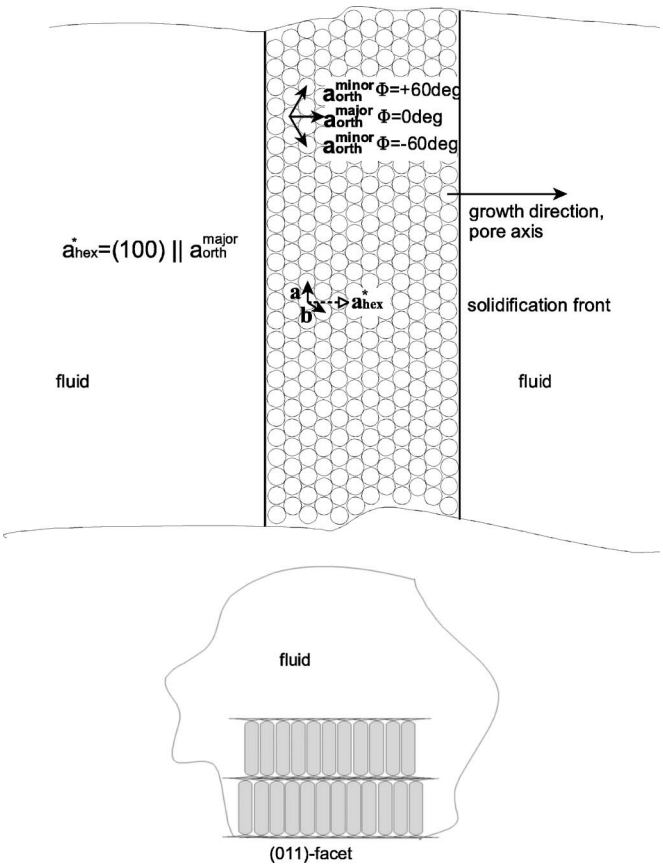

FIG. 10. Schematic picture of the solidification process of alkanes in mesopores. The upper panel shows a side view of the pores, along the axes of the alkane molecules, the lower panel the pore cross section with molecules standing on a (011) facet, such that the alkane layers are parallel to this part of the pore wall.

Adsorption isotherms of Ar in porous Si and porous glasses at temperatures below the triple point of the pore filling show that the vapor pressure at which pore solid forms is close to but still slightly below the saturated vapor pressure of bulk sublimation [3,24]. This proves directly that the Ar pore solid is stable (but only marginally so). Such experiments are, however, not feasible on the alkanes of this study, because of the low vapor pressure below their melting points.

Nevertheless one can come up with definite conclusions on the stability of the alkane solid confined in porous Si by comparing results obtained on freshly prepared substrates and on substrates that have been oxidized by a subsequent treatment with peroxide. Doing so, the infrared spectrum changes. The absorption bands of the vibrations of the terminal Si-H groups are replaced by those of Si-O-H groups. In fact the oxidation process can be continued to completion by baking in air upon which the porous sheets finally turn transparent to visible light.

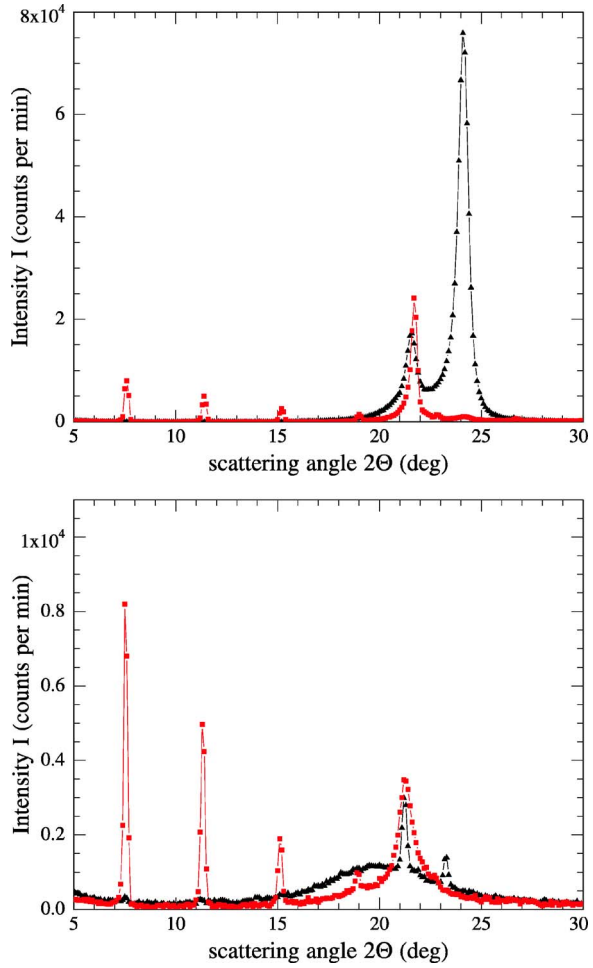

FIG. 11. (Color online) Diffraction patterns of C17, obtained by scans along q_p, at 250 (upper panel) and 291 K (lower panel). Results on the oxidized substrates (squares) and on the nonoxidized subtrates (triangles) are compared.

For both types of samples the liquid is sucked into the pores, and the pore liquid is stable in both cases. Diffraction patterns on C17 have been recorded for both types of substrate. They are different, as is illustrated in Fig. 11 for $T=250$ and 291 K. The results shown are scans along q_p, i.e., in reflection geometry. At 250 K, well in the solid regime, the data on the nonoxidized sample show the usual (111)-(11$\bar{1}$) and (200) doublet (see also Fig. 6), whereas in the oxidized sample, the (200) peak is practically absent and the (00l) series shows up instead. Furthermore, the diffraction peaks obtained on the oxidized substrate are sharper; their width is given by the instrumental resolution. One concludes that the alkane has left the pores and exists as bulk solid on the external surface of the sample, with some preference for the alkane layers to be parallel to the surface of the sample. The second pair of diffraction patterns has been recorded at 291 K. This is just the melting point of pore confined C17, but already well below the the melting point of bulk C17. Accordingly, the pattern obtained on the oxidized substrate shows the Bragg peaks of the solid state, similar to what has already been observed at 250 K, whereas the pattern on the nonoxidized sample indicates liquid-solid coexistence, the liquid phase being represented by the broad first maximum of the structure factor. One concludes that the alkane in the oxidized pores eventually turns unstable on cooling. It then flows out of the pores and forms a bulk solid on the surface of the sample. Solid C17 is unstable in the oxidized pores, but obviously stable in the nonoxidized pores. The different behavior points to some reduction of the molecule-substrate interaction upon oxidation. The C17 molecule is a nonpolar molecule, hence the interaction is mainly of van der Waals type. Obviously such interactions are reduced by the slight oxidation of the substrate. It would be interesting to study how *n*-alcohols would respond to the oxidation of the substrate since these molecules would interact with the oxide by means of dipolar forces and H bonds.

Having said so, one wonders why the solid alkanes are stable in porous glasses. The glasses are practically pure SiO_2 and are, so to say, what one gets after complete oxidation of porous Si. We do not have a straight answer. Is it really that the molecules are oriented differently with respect to the pore axis? Or does the topology of the pore space matter? In porous Si the pore filling is an ensemble of independent linear, quasi-one-dimensional objects, whereas in the glasses the pores are multiply connected and in this sense the filling is a spongelike object with macroscopic dimensions in all three directions of space. Ideas along this line have been formulated in context with the (hysteretic) vapor-liquid transition in pores which is usually probed by the measurement of vapor pressure isotherms [25].

VI. SUMMARY

The medium length *n*-alkanes C16, C17, C19, and C25 have been embedded in porous Si with a pore diameter of 10 nm. The melting transition is reduced with respect to the bulk state and there is thermal hysteresis between freezing and melting. Analogous observation have been made of a large number of molecules in mesopores. Not only is the existence range of the liquid state increased by the confinement but also that of the mesophases. For C16 even a mesophase appears that is absent in the bulk state.

Almost the entire solidified pore filling exists in six discrete domains that have special crystallographic orientations with respect to the lattice of the Si host. This is the central result of our study. The orientations are brought forth by the propagation of the solidification front with the (three equivalent) directions of fastest growth parallel to the pore axis. One can speak of a nanoscale version of the Bridgman technique of single-crystal growth. As a result of this selection process the pore axis lies in the plane of the alkane layers, with the consequence that the molecules are perpendicular to the pore axis. At lower temperatures the two of the six orientation states develop into majority domains that have the orthorhombic *a* direction, the direction of strongest thermal contraction, coinciding with the pore axis. Furthermore, there is also a strong texture with respect to the rotation angle about the pore axis that is consistent with the fourfold symmetry of the pore axis in reference to the Si lattice. This is surprising since the pore cross section does not reflect this symmetry.

Finally, we have shown that the alkane solid is thermodynamically stable in porous Si, but unstable if the pore walls are slightly oxidized.

For the future it would be interesting to explore how the structure of the pore solid is affected by details of the molecule–pore-wall interaction. For example, studies on the molecular arrangement at *n*-alkane/Al_2O_3 (sapphire) interfaces indicate a parallel alignment of the long axes of *n*-alkane molecules to the sapphire surface, whereas, upon silanization, the tendency for this preferred orientation is reduced significantly [26,27]. Thus, silanizing the pore walls or gradual increasing the thickness of the oxide layer at the pore wall may lead to a substantially altered crystallization and thermodynamical behavior compared to the one presented in this study.

ACKNOWLEDGMENTS

We thank J. Schmauch for taking the electron microscope images and R. Berwanger for the infrared measurements. The work has been supported by the Deutsche Forschungsgemeinschaft via the Sonderforschungsbereich 277, Saarbrücken.

[1] H. K. Christenson, J. Phys.: Condens. Matter **13**, R95 (2001).
[2] C. Alba-Simionesco, B. Coasne, G. Dosseh, G. Dudziak, K. E. Gubbins, R. Radhakrishnan, and M. G. Sliwinska-Bartkowiak, J. Phys.: Condens. Matter **18**, R15 (2006).
[3] P. Huber and K. Knorr, Phys. Rev. B **60**, 12657 (1999).
[4] P. Huber, D. Wallacher, J. Albers, and K. Knorr, Europhys. Lett. **65**, 351 (2004).
[5] D. Wallacher, R. Ackermann, P. Huber, M. Enderle, and K. Knorr, Phys. Rev. B **64**, 184203 (2001).
[6] E. B. Sirota, H. E. King, Jr., D. M. Singer, and Henry H. Shao, J. Chem. Phys. **98**, 5809 (1993).
[7] E. B. Sirota and A. B. Herhold, Science **283**, 529 (1999).
[8] J. Doucet, I. Denicolo, and A. Craievich, J. Chem. Phys. **75**, 1523 (1981).
[9] J. Doucet, I. Denicolo, A. Craievich, and A. Collet, J. Chem. Phys. **75**, 5125 (1981).
[10] M. Dirand, M. Bouroukba, V. Chevallier, D. Petitjean, E. Behar, and V. Ruffier-Meray, J. Chem. Eng. Data **47**, 115 (2002).
[11] P. Huber, V. P. Soprunyuk, and K. Knorr, Phys. Rev. E **74**, 031610 (2006).
[12] R. Montenegro and K. Landfester, Langmuir **19**, 5996 (2003).
[13] B. Xie, H. Shi, S. Jiang, Y. Zhao, C. C. Han, D. Xu, and D. Wang, J. Phys. Chem. B **110**, 14279 (2006).
[14] M. Okazaki, K. Toriyama, and S. Anandan, Chem. Phys. Lett. **401**, 363 (2005).
[15] J. Salonen, V. P. Lehto, and E. Laine, Appl. Phys. Lett. **70**, 637 (1997).
[16] Y. H. Ogata, T. Tsuboi, T. Sakka, and S. Naito, J. Porous Mater. **7**, 63 (2000).
[17] A. E. Pap, K. Kordas, G. Toth, J. Levoska, A. Uusimaki, J. Vahakangas, S. Leppavuori, and T. F. George, Appl. Phys. Lett. **86**, 041501 (2005).
[18] V. Lehmann and U. Gösele, Appl. Phys. Lett. **58**, 856 (1991); V. Lehmann, R. Stengl, and A. Luigart, Mater. Sci. Eng., B **69–70**, 11 (2000).
[19] E. S. Domalski and E. D. Hearing, and J. Phys. Chem. Ref. Data **251**, 1 (1996).
[20] A. A. Schaerer, C. J. Busso, A. E. Smith, and L. B. Skinner, J. Am. Chem. Soc. **77**, 2017 (1955).
[21] M. Maroncelli, S. P. Qi, H. L. Strauss, and R. G. Snyder, J. Am. Chem. Soc. **104**, 6237 (1982).
[22] S. C. Nyburg, F. M. Pickard, and N. Norman, Acta Crystallogr., Sect. B: Struct. Crystallogr. Cryst. Chem. **32**, 2289 (1976).
[23] K. Knorr, D. Wallacher, P. Huber, V. Soprunyuk, and R. Ackermann, Eur. Phys. J. E **12**, 51 (2003).
[24] T. Hofmann, D. Wallacher, P. Huber, and K. Knorr, J. Low Temp. Phys. **140**, 91 (2005).
[25] E. Kierlik, P. A. Monson, M. L. Rosinberg, L. Sarkisov, and G. Tarjus, Phys. Rev. Lett. **87**, 055701 (2001); D. Wallacher, N. Künzner, D. Kovalev, N. Knorr, and K. Knorr, *ibid.* **92**, 195704 (2004).
[26] M. S. Yeganeh, Phys. Rev. E **66**, 041607 (2002); K. Nanjundiah and A. Dhinojwala, Phys. Rev. Lett. **95**, 154301 (2005).
[27] Mohsen Yeganeh (private communication).